Article:
Pope, S.A., Gedalin, M. and Balikhin, M.A. (2019) The first direct observational confirmation of kinematic collisionless relaxation in very low mach number shocks near the Earth. Journal of Geophysical Research: Space Physics, 124 (3). pp. 1711-1725. ISSN: 2169-9402

https://doi.org/10.1029/2018ja026223

JGR Space Physics

RESEARCH ARTICLE
10.1029/2018JA026223

The First Direct Observational Confirmation of Kinematic Collisionless Relaxation in Very Low Mach Number Shocks Near the Earth

S. A. Pope[1], **M. Gedalin**[2], **and M. A. Balikhin**[1]

[1]Department of Automatic Control and Systems Engineering, University of Sheffield, Sheffield, UK, [2]Department of Physics, Ben-Gurion University, Beer-Sheva, Israel

Key Points:
- The first correlative analysis of simultaneous measurements of the magnetic field and plasma at shocks near to the Earth is presented
- The first direct observational confirmation of kinematic collisionless relaxation is presented
- A clear separation of the contribution of protons and of alpha particles is found

Correspondence to:
S. A. Pope,
s.a.pope@sheffield.ac.uk

Citation:
Pope, S. A., Gedalin, M., & Balikhin, M. A. (2019). The first direct observational confirmation of kinematic collisionless relaxation in very low mach number shocks near the Earth. *Journal of Geophysical Research: Space Physics*, *124*, 1711–1725. https://doi.org/10.1029/2018JA026223

Received 22 OCT 2018
Accepted 27 FEB 2019
Accepted article online 8 MAR 2019
Published online 22 MAR 2019

Abstract Collisionless shocks are ubiquitous throughout the known universe. They mainly convert the energy of the directed ion flow into heating. Upon crossing the shock front, the ion distribution becomes nongyrotropic. Relaxation to gyrotropy then occurs mainly via kinematic collisionless gyrophase mixing and interaction with waves. The theory of collisionless relaxation predicts that the downstream pressure of each ion species varies quasi-periodically with the distance from the shock transition layer and the amplitude of the variations gradually decrease. The oscillations due to each species have their own spatial period and damping scale. Pressure balance requires that the variations in the total plasma pressure should cause anticorrelating variations in the magnetic pressure. This process should occur at all Mach numbers, but its observation is difficult at moderate-/high-Mach numbers. In contrast, such magnetic oscillations have been observed at low Mach number cases of the Venusian bow shock and interplanetary shocks. In this paper, simultaneous in situ magnetic field and plasma measurements from the THEMIS-B and THEMIS-C spacecraft are used to study, for the first time, the anticorrelated total ion and magnetic pressure spatial variations at low-Mach number shocks. It is found that kinematic collisionless relaxation is the dominant process in the formation of the downstream ion distribution and in shaping the downstream magnetic profile of the observed shocks, confirming fundamental theoretical results. Comparison with the results from numerical models allows the role of the different ion species to be investigated and confirms the role heavy ions play in forming the downstream magnetic profile.

1. Introduction

Collisionless shocks are believed to be one of the most efficient particle acceleration processes in the known universe and capable of accelerating charged particles to some of the highest known energies (in excess of 10^{15} eV; Helder et al., 2012; Schure et al., 2012; Van Weeren et al., 2010). They also play an important role in planetary interaction with the solar wind (e.g., Russell, 1985), and it is only within the solar system that in situ observations can be made. In particular, it is only around the Earth where substantial and coordinated multipoint observations using high-quality magnetic, electric, and plasma measurements have been conducted (e.g., Balogh et al., 2005; Burch et al., 2016; Galeev et al., 1996; Ogilvie et al., 1977; Sibeck & Angelopoulos, 2008).

A collisionless shock forms whenever a supermagnetosonic flow encounters an obstacle and is decelerated to a submagnetosonic speed. In the shock frame the energy of the directed ion flow is redistributed by the shock into ion heating, electron heating, magnetic field amplification, and acceleration of a small fraction of particles to high energies. Since it is ions that mainly shape the shock profile, the downstream ion distributions and magnetic profile are intimately related. Collisionless shocks are typically classified by the angle between the shock normal and the upstream magnetic field θ_{Bn}, the Alfvén Mach number $M_A = v_{u,x}/v_A$ (the ratio of the upstream flow velocity $v_{u,x}$ in the shock normal direction to the Alfvén speed v_A), and the upstream ratio of the kinetic-to-magnetic pressure $\beta = 8\pi n_u T_u/B_u^2$ (n_u is the upstream number density, B_u is the upstream magnetic field magnitude, and T_u is the upstream temperature). Different species can have different upstream temperatures, so that each species has its own β. Understanding the key energy redistribution processes for the different categories of shocks is one of the most important problems in the study of collisionless shocks.

Quasi-perpendicular shocks with $\theta_{Bn} \gtrsim 45°$ usually have a well-structured magnetic field profile (Burgess et al., 1989; Kennel et al., 1985; Mellott, 1985; Scudder et al., 1986). With the increase of the Mach number the magnetic compression also increases, and some ions become reflected and appear ahead of the ramp (the steepest magnetic field increase in the shock transition layer). The number of reflected ions increases with the increase of the Mach number, together with their effect on the shock structure (e.g., Scudder et al., 1986). Upon crossing the ramp toward downstream, the reflected ions represent a superthermal population. The ion thermalization downstream of the magnetic ramp is a result of the joint gyration of transmitted and reflected ion populations. The role of reflected ions is substantial in high-Mach number shocks, and reflected ions have been detected ahead of subcritical shocks (Greenstadt & Mellott, 1987). However, they do not play a significant role in low-Mach number subcritical shocks. For low-Mach number shocks, it was believed that anomalous interaction with waves generated within the shock front would lead to the redistribution of the kinetic energy of the directed upstream flow into other degrees of freedom and consequently to ion heating. Ion sound waves generated by the electric current associated with the gradient of the magnetic field within the front were employed by many models for anomalous processes at the shock front (e.g., Galeev, 1976). While it has been understood for some time that "the coherent forces within the shock layer" (Scudder, 1995) are the most efficient mechanism for redistribution of energy at supercritical shocks, it was assumed that anomalous processes are key to such redistribution in weak subcritical shocks.

The theory of low-Mach number collisionless shocks was thought to be well understood (Kennel et al., 1985), until an observation of a new type of very low Mach number quasi-perpendicular collisionless shock and the development of an associated theory (Balikhin et al., 2008; Ofman et al., 2009). Classical dissipative low-Mach number shocks do not exhibit any visible oscillatory structure ahead of the ramp, while dispersive low-Mach number shocks exhibit a wave precursor ahead of the shock ramp for the quasi-perpendicular case and a trail of waves downstream of the shock for the perpendicular case ($\theta_{Bn} \gtrsim 88.5°$). The magnetic profile of both types of quasi-perpendicular low-Mach number shock has a smooth transition across the ramp and does not exhibit an overshoot or any downstream oscillations. However, the very low Mach number quasi-perpendicular shocks observed by Balikhin et al. (2008) using magnetic field measurements made by Venus Express exhibited oscillations in the magnetic field downstream of the shock ramp. Balikhin et al. (2008) proposed that these oscillations were due to the kinematic relaxation of the downstream nongyrotropic ion population and supported this with theory and numerical analysis based on the previously developed theory of gyrating downstream ion distributions (Gedalin, 1996, 1997; Zilbersher et al., 1998).

Kinematic relaxation is the main mechanism for the formation of the downstream ion distribution in all magnetized shocks. Nongyrotropy of the downstream ions results in the spatially dependent ion pressure, which, in turn, requires that the magnetic pressure is spatially dependent in the opposite phase, unless the shock front is significantly time dependent (Gedalin, 2015). For an incident upstream ion distribution with a noncold temperature distribution, the downstream distribution of the ion velocities leads to a gradual mixing of the plasma as the ions gyrate and drift. This leads to a reduction and eventually the elimination of the downstream oscillations when the ion distribution is homogenized. In high-Mach number shocks, the reflected and directly transmitted ions gyrated differently, and the resulting downstream oscillations of the magnetic field are not periodic and may even look unordered (Gedalin, 2016; Ofman & Gedalin, 2013). In low-Mach number high-β shocks the relaxation is fast so that often only an overshoot may be observed (Gedalin, 2015; Gedalin et al., 2015). In low-Mach number low-β shocks the influence of the reflected ions is expected to be negligible (Gedalin, 2016), the relaxation length is expected to be large, and the downstream oscillations are expected to be nearly periodic (Gedalin, 2015). Such shocks are, therefore, the best candidates for observations of kinematic collisionless relaxation and direct comparison with the theory. Balikhin et al. (2008) refers to such low-Mach number low-β shocks as "kinematic," in the same way that other shocks are classed as resistive or dispersive due to the dominating physical mechanism, even if other mechanisms are present.

Ofman et al. (2009) presented further theoretical analysis and hybrid simulation of these very low Mach number shocks observed at Venus. They compared them to other very low and low Mach number shocks (similar to those observed by Farris et al., 1993), in terms of the upstream conditions and presence of a nongyroptropic downstream ion population. The conclusion was that very low Mach number, low β, and quasi-perpendicular conditions are the most favorable for the observation of oscillations associated with nongyrotropic ions. Following the discovery by Balikhin et al. (2008), oscillations in the downstream magnetic field have also been observed for low Mach number interplanetary shocks (Kajdič et al., 2012;

Russell et al., 2009). Goncharov et al. (2014) used nonsimultaneous magnetic field measurements from Wind and plasma measurements from Spektr-R to study low to moderate Mach number interplanetary shocks. Downstream oscillations suggestive of kinetic processes were observed in a number of shocks, but they did not directly show the anticorrelated oscillations in the magnetic and ion pressures predicted by theory.

Additional insight into the conditions associated with the generation of these very low Mach number shocks where the kinematic effects can be seen most clearly can be gained from other studies using Venus Express data. Zhang et al. (2008) analyzed a very strong interplanetary coronal mass ejection (ICME), which occurred at the same time as the shocks analyzed by Balikhin et al. (2008). This ICME had a magnetic field strength approximately twice the magnitude of a typical ICME at 0.72AU. This resulted in a very dynamic and abnormally high altitude bow shock, which was associated with the very low Mach number of the solar wind during this period. Vech et al. (2015) presented a statistical study of the interaction of ICMEs with Venus using both magnetic field and plasma measurements and included the ICME previously analyzed by Zhang et al. (2008). They found that under most conditions the position of the bow shock is not significantly affected by an ICME. However, higher locations were correlated with the passage of the magnetic cloud phase of an ICME (the region following the ICME shock front and sheath). In addition to a smoothly rotating abnormally large magnetic field for the solar wind, they are characterized by a diminished proton temperature and often low proton densities (Burlaga et al., 1981; Leamon, 2002). While the lower proton temperature acts to lower the velocity of sound in the plasma, a lower density contributes to a raised Alfvén velocity. Consequently, since the magnetic field is abnormally large, the Alfvén velocity dominates the magnetosonic velocity. Thus, if the solar wind velocity associated with the ICME is not particularly large, the Mach number in the magnetic cloud phase of the ICME will be exceptionally small. Ofman et al. (2009) suggested that the best conditions for the observation of the oscillations in the magnetic field due to ion nongyrotropy are when both the wave activity and ion temperature are low. These are conditions that are also associated with the cloud phase of an ICME.

Previous studies have found that the jump in magnetic field across the bow shock at Venus is smaller than at the terrestrial shock (Lu et al., 2013; Russell et al., 1979). It was argued that pickup ions are the main mechanism causing this reduction. This suggests that the Mach number of the shocks observed by Balikhin et al. (2008) might not be as small as determined from the magnetic field data alone. However, the effect of pickup ions appears to be asymmetric. Near the terminator, pickup ions appear to play an important role, but in the near-subsolar ($35° < SZA < 75°$) region their influence appears less important (Chai et al., 2015). The shocks observed by Balikhin et al. (2008) occur in the near-subsolar region ($SZA = 67 - 68°$), suggesting that pickup ions play a less important role in the observed shocks than would be the case at other locations. McEnulty et al. (2010) also show that ICMEs do not have a noticeable effect on pickup ion flux, indicating that the nontypical solar wind conditions, which occurred when Balikhin et al. (2008) made these observations, should not lead to the presence of a radically different amount of pickup ions. Despite this, pickup ions cannot be ruled out as contributing to the structure of the unusual very low Mach number shocks previously observed at Venus.

The numerical analysis in Balikhin et al. (2008) showed that oscillations of the downstream ion population create a total plasma pressure profile that is out of phase with the oscillations in the magnetic pressure, leading to the total pressure balance required. However, as no plasma measurements were available for this time period, this theory could not be validated. Even if plasma measurements were available for Venus Express, they would unlikely be of sufficient temporal resolution to allow validation of the theory. In this paper, observations of very low Mach number terrestrial shocks with very similar characteristics to those observed at Venus by Balikhin et al. (2008) are presented. The terrestrial shocks also occur during the magnetic cloud phase of an ICME. The availability of simultaneous THEMIS-C magnetic field and plasma data allows the solar wind, downstream conditions, and shock structure to be examined in much more detail than was possible using Venus Express data. The results verify the theory previously proposed for the formation of such very low Mach number shocks and suggest that they are widespread when the required conditions prevail. Recent theoretical work has shown that α particles may affect the downstream magnetic profile by "spoiling" periodicity of oscillations and adding a second period (Gedalin, 2017a, 2017b). The conditions of the THEMIS-C observations also allow us to test these predictions.

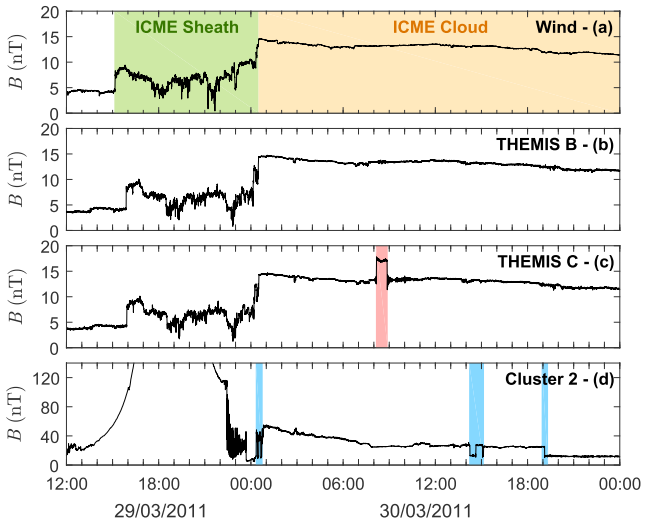

Figure 1. Wind (a), THEMIS-B (b), THEMIS-C (c), and Cluster 2 (d) spin-rate fluxgate magnetometer magnitude data from 15:00 on 29 March 2011 to 20:00 on 30 March 2011. Panel (a) shows that Wind encounters an interplanetary coronal mass ejection (ICME) following a period of relatively nominal solar wind conditions. The green-shaded region in panel (a) marks the sheath phase of the ICME. This is followed by the cloud phase of the ICME, which marked by the orange-shaded region. Panels (b) and (c) show that THEMIS-B and THEMIS-C also encounter the ICME, with a delay of approximately 45 min compared to Wind. THEMIS-B remains in the solar wind for the entirety of the period plotted. In contrast, the red-shaded region marks the period when THEMIS-C briefly moves across a shock into the downstream region. Panel (d) shows that after traveling out from the magnetosphere at the end of 29 March 2011, Cluster 2 is initially in the solar wind at the start of 30 March 2011 and just before the ICME reaches the Earth. Just as the ICME reaches the Earth, Cluster 2 crosses the bow shock several times over a short period (first blue-shaded region) before remaining in the magnetosheath until several further crossing of the bow shock (second and third blue-shaded regions), after which it remains in the solar wind.

2. Data and Observations

The ARTEMIS mission is composed of the THEMIS-B and THEMIS-C spacecraft, which, following the end of the nominal phase of the THEMIS mission in 2010, were moved to a near Lunar orbit (Angelopoulos, 2011). This combination of orbit and THEMIS instrumentation makes the ARTEMIS mission suitable to study the Earth's bow shock when it is unusually distant from the planet. Figure 1 shows the magnetic field measured by Wind (a), THEMIS-B (b), THEMIS-C (c), and Cluster 2 during an ICME. The leading shock of an ICME is detected by Wind on 29 March 2011 at just after 15:00 UT and is followed by the ICME sheath (green-shaded region) and then the magnetic cloud phase (orange-shaded region). The magnetic cloud was was characterized by a slowly rotating magnetic field with a large magnitude (~12–14 nT compared to 2- to 4-nT upstream of the ICME) with less short term fluctuations, an ion number density of about the same or less than the normal solar wind levels (usually around ~1–5 cm^{-3} total ion density compared to 3–5 cm^{-3} upstream of the ICME) and a total ion speed greater than upstream of the ICME (~340–360 km/s in the ICME cloud compared to ~310–330km/s upstream of the ICME). During this period THEMIS-B and THEMIS-C were positioned in the dayside solar wind and also detected the leading shock associated with the ICME just before 16:00 UT, approximately 45 min after Wind, and this was followed by a similar sheath and magnetic cloud phases. Comparison between Wind and THEMIS-B magnetic field magnitude data shows a very similar profile. However, the red band in Figure 1c shows that during the ICME cloud phase, THEMIS-C also crossed a shock, first at 08:09:40 UT into the downstream region and then at 08:51:40 UT back into the upstream region. The location of THEMIS-C was [32, −49, 4] R_E during this period, while THEMIS-B was positioned slightly upstream at [40, −42, 4] R_E. For comparison Cluster 2 crosses the Earth's bow shock multiple times during the ICME, as shown by the blue bars in Figure 1d, and is located in the dayside magnetosheath at [15, −1, −9] R_E during the THEMIS-C shock crossings.

Figure 2 shows the shock crossings measured by THEMIS-C in the magnetic field and on-board derived ion moment data. The on-board derived moments are the only THEMIS-C data that contains a complete set of spin-rate plasma moments for 30 March 2011. Throughout this paper, unless otherwise stated, the normal, noncoplanar, and coplanar shock geometry components are indicated by x, y, and z, respectively, while the

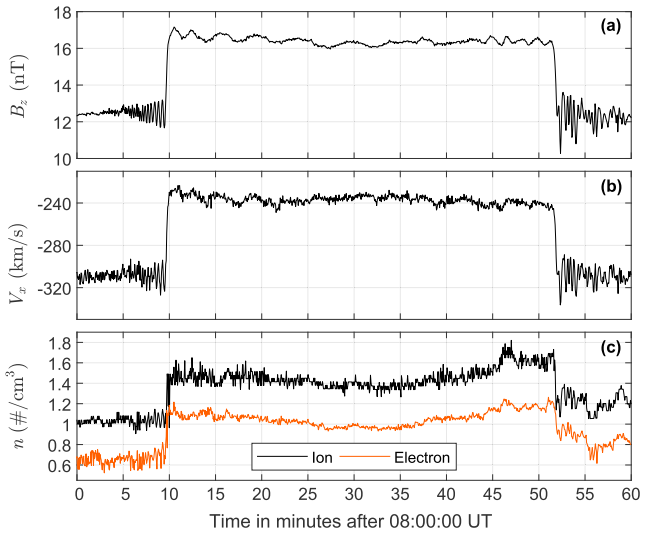

Figure 2. THEMIS-C magnetic field data projected into the coplanar direction for the inbound shock normal (a), ion velocity projected along the inbound shock normal (b), and ion (black) and electron (red) number density (c) for the period marked by the red bar in Figure 1c, that is, from just before THEMIS-C first crosses the shock at 08:10 UT, until just after it crosses the shock again at 08:52 UT into the upstream region. The shock normal is determined using the double coplanarity method. The shock is clearly seen in the jump in all three quantities.

prefix GSE is used to distinguish geocentric solar ecliptic coordinates. The shock crossings are clearly seen in the jump in the shock frame coplanar component of the magnetic field (a), ion velocity in the shock normal direction (b), and particle density (c). However, for the regions upstream of the two shock crossings and within the magnetosphere, $n_i > n_e$ in the THEMIS-C density data. This violates quasi-neutrality for the solar wind and the amount that $n_i > n_e$ is significant enough to suggest that the data are not accurate. The source of this inaccuracy is likely due to the particle beam size in the solar wind and the operating mode of the electrostatic analyzer used during this period of measurement (McFadden, Carlson, Larson, Bonnell, et al., 2008; McFadden, Carlson, Larson, Ludlam, et al., 2008). In contrast both THEMIS-B (which is positioned close to THEMIS-C) and Wind data have $n_i < n_e$ throughout the magnetic cloud, as would be expected for a neutral plasma with an α-particle or heavy ion component. THEMIS-B and Wind (adjusted with a 45-min delay to compensate for the propagation of the ICME from Wind to THEMIS-B) are also consistent and agree well. Both suggest that $n_i \approx 0.7$ cm^{-3} upstream of the shock crossings, as opposed to $n_i \approx 1$ cm^{-3} measured by THEMIS-C, and both indicate that the ratio of α particles to protons n_α/n_p is most likely in the region of 0.02–0.06. In contrast, THEMIS-B and THEMIS-C ion velocity measurements in the magnetic cloud show good agreement. It should be noted that the theoretical-numerical approach used in section 3 is capable of providing sufficient detail for comparison with observations even if some data are missing. In this way the theory allows the gaps in measurements to be filled. The Wind measured α particle to proton density ratio (see Figure 3) shows variability at the time scale of minutes. Wind is actually quite a long way from the vector projecting away from THEMIS-C along the direction of the solar wind velocity. However, as the magnetic cloud is a very large structure occurring from the same source region on the solar surface, the Wind n_α/n_p should reflect observations at THEMIS-C. ACE is positioned much closer to this vector, but only preliminary and not final product data are available for the period of interest. By using the Wind observations of $n_\alpha/n_p = 0.02$–0.04 as an initial indicator, our approach described in section 3 allows us to evaluate the n_α/n_p, which is most consistent with the THEMIS-C observations.

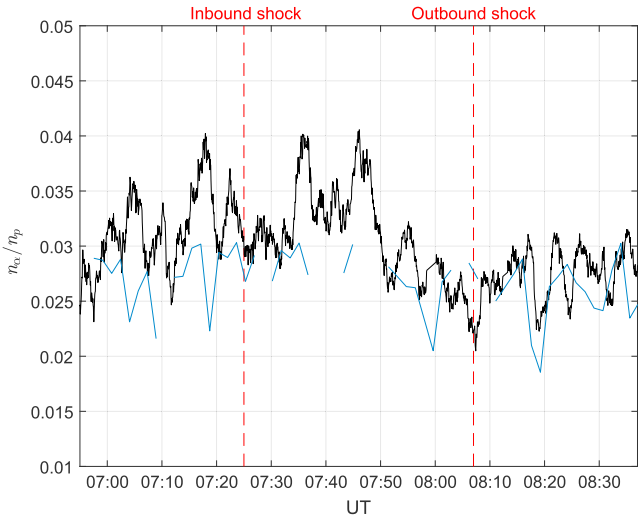

Figure 3. Wind measured α particle to proton density ratio showing variability at the time scale of minutes. The black line is calculated from the 3DP ion moments using a window size of 30 to remove high-frequency fluctuations. The blue line is the solar wind experiment values determined using nonlinear fitting and moments. The two dashed red lines show the time of the THEMIS-C bow shock crossings shifted by 45 min to compensate for the solar wind propagation time from Wind to THEMIS-C.

Table 1
Shock Normal Direction (GSE) and θ_{Bn} Determined Using Four Different Methods for the Inbound and Outbound Shock Xrossings

Method	Inbound shock		Outbound shock	
Model (Peredo et al., 1995)	[−0.88, 0.47, −0.04]	78°	[−0.88, 0.47, −0.04]	77°
Minimum variance	[−0.95, 0.32, 0.03]	73°	[−0.90, 0.43, 0.01]	74°
Magnetic coplanarity	[−0.90, 0.44, 0.09]	70°	[−0.67, 0.72, 0.18]	67°
Double coplanarity	[−0.92, 0.38, 0.08]	71°	[−0.90, 0.41, 0.10]	69°

Note. GSE = geocentric solar ecliptic.

Several methods have been used to calculate the shock normal direction. Table 1 shows the shock normal direction and θ_{Bn} determined using the model shock normal (Peredo et al., 1995) scaled to the observed shock location, minimum variance (magnetic field data), coplanarity (magnetic field data), and double coplanarity (magnetic field and ion velocity data). Due to the apparent inaccuracy in the ion density data, the Rankine-Hugoniot conditions are not used to determine the shock normal. For very low Mach number shocks, the minimum variance technique can be prone to error due to the small noncoplanar magnetic field. For this reason, together with the consistency between the calculated inbound and outbound normal and reliance on both magnetic field and ion velocity measurements, the double coplanarity shock normals are used throughout this paper. However, for the analysis that follows, use of the minimum variance normal leads to very similar results.

The inbound and outbound shocks have θ_{Bn} values of 71° and 69°, respectively, indicating that they are both quasi-perpendicular shocks. The shocks presented by Balikhin et al. (2008) had shock normals of 70–80°. Figure 4 shows the inbound and outbound shock crossings in the normal incidence frame (NIF) resulting directly from the double coplanarity method. From Figures 3a and 4, it is evident that both the inbound and outbound shock crossings exhibit the same low-frequency downstream oscillations in the magnetic field, which was observed in the shocks presented by Balikhin et al. (2008). The low-frequency downstream oscillations are linearly polarized along the mean magnetic field (the angle between the maximum variance direction and mean downstream field is <0.5° and the eigenvalue ratio $\lambda_{max}/\lambda_{int} > 500$ for both shocks).

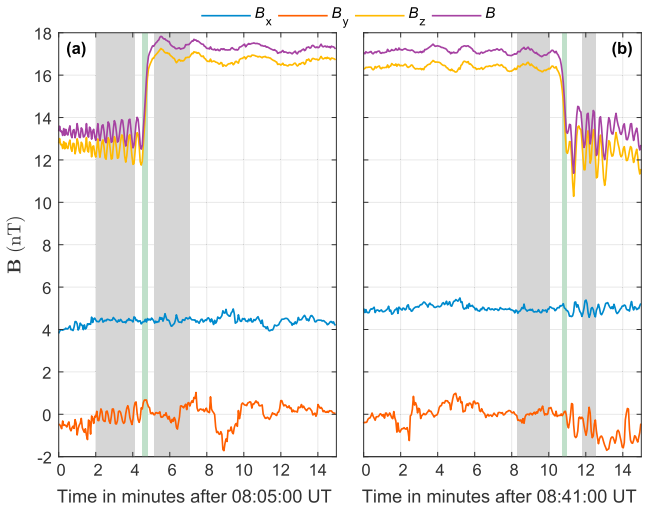

Figure 4. THEMIS-C spin-rate magnetic field data rotated into the normal incidence frame for the inbound (a) and outbound (b) shock crossings. The normal incidence frame is determined using the double coplanarity method. The blue line is the normal component, the red line is the noncoplanar component, the yellow line is the main coplanar component, and the purple line is the total magnetic field. The gray regions mark the upstream and downstream regions used for the calculation of any average values in this paper. The green region marks the shock ramp. Linearly polarized waves in the coplanar direction, which is also approximately parallel to the direction of the magnetic field, are observed downstream of both shocks. Upstream of the inbound shock (a), waves elliptically polarized in the plane of the shock front are observed. Similar waves are observed upstream of the outbound shock (b), but the polarization is not quite in the plane of the shock front.

These observations are consistent with those of Balikhin et al. (2008) and the kinematic relaxation of the downstream ion population.

Due to the lack of multiple spacecraft measurements, the inaccurate density measurements, and the small angle between the upstream and downstream ion velocities, none of the conventional methods for determining the shock velocity V_{sh} are likely to provide a reliable result (Schwartz, 1998). However, for the observed shocks an alternative approach exists to estimate the shock velocity. The wavelength of the downstream kinematic oscillations for a cold plasma is predicted by theory to be equation (1) (Balikhin et al., 2008; Ofman et al., 2009), with u and d denoting average upstream and downstream values, respectively, and x denoting the direction along the shock normal for velocities in the NIF. $r_{u,i}$ is the upstream ion convective gyro-radius and defined in equation (2) as the ratio of the upstream normal velocity in the NIF to the upstream ion-cyclotron frequency. For kinematic oscillations polarized along the shock normal, the shock velocity can be calculated by equation (5), that is, the wavelength of the downstream oscillations divided by the time to traverse a single oscillation Δt.

$$l_d = 2\pi r_{i,u} \frac{V_{d,x}}{V_{u,x}} \frac{B_u}{B_d}, \tag{1}$$

$$r_{i,u} = \frac{V_{u,x}}{\Omega_{u,i}}, \tag{2}$$

$$\hat{\mathbf{n}} \cdot V_{sh} = \frac{l_d}{\Delta t}. \tag{3}$$

Since the velocities in equations (1) and (2) are in the NIF, they are also a function of the shock velocity V_{sh}, that is, equation (4).

$$\begin{aligned} V_x &= \left(\left(\mathbf{V}_{GSE} + \mathbf{V}_{sh}\right) - \hat{\mathbf{n}} \times \left(\left(\mathbf{V}_{GSE} + \mathbf{V}_{sh}\right) \times \hat{\mathbf{n}}\right)\right) \cdot \hat{\mathbf{n}} \\ &= \left(\mathbf{V}_{GSE} + \mathbf{V}_{sh}\right) \cdot \hat{\mathbf{n}}. \end{aligned} \tag{4}$$

Solving equations (1)–(4) to get V_{sh} leads to equation (5), which is a function of the downstream magnetic field magnitude, ion velocity vector in the GSE frame, the shock normal direction, and the time to traverse a single downstream oscillation.

$$\begin{aligned} \hat{\mathbf{n}} \cdot V_{sh} &= \frac{k}{1-k} \hat{\mathbf{n}} \cdot \mathbf{V}_{GSE,d}, \\ k &= \frac{2\pi}{\Omega_{d,i} \Delta t}. \end{aligned} \tag{5}$$

Table 2 contains the relevant measured or calculated average upstream u and downstream d parameters used in the analysis of the inbound and outbound shock crossing. Using these average values, the time to traverse the first complete oscillation downstream of each shock crossing, and assuming that the observed oscillations are due to protons, the resulting shock velocities are 8.3 km/s sunward for the inbound shock and 10.9 km/s antisunward for the outbound shock. The wavelength of the proton kinematic oscillations is 940 km (3.5 upstream ion convective gyro-radii) and 896 km (3.8 upstream ion convective gyro-radii) for the inbound and outbound shocks, respectively. It is apparent from Figure 1d that the period of the downstream oscillations changes. This phenomena is investigated further using numerical analysis techniques later in this paper.

Both of these shock crossings have low magnetic compression. The increase across the ramp for the inbound and outbound shocks is 0.31 and 0.27 B_u, respectively, which is comparable to the magnetic compression of $0.3B_u$ for the shocks observed by Balikhin et al. (2008). The upstream Alfvén Mach numbers estimated from the magnetic field data using $M_A \approx \sqrt{R(R+1)/2}$, where $R = B_d/B_u$ and which is valid for a cold perpendicular shock (Gedalin et al., 2015), are 1.21 and 1.23 for the inbound and outbound shock, respectively. The values calculated directly using the THEMIS-C magnetic field and on-board plasma data using a two-fluid assumption with $n_\alpha/n_p = 0.04$ for both the inbound and outbound shock and correcting for the effect of heavy ions in the THEMIS-C velocity and density data, which is measured as a proton only plasma

Table 2
Measured and Calculated Parameters for the Inbound and Outbound Shocks Using the the Flux-Gate Magnetometer Magnetic Field Data and on-Board Derived THEMIS-C Plasma Moments (Unless Otherwise Stated in the Main Body)

Parameter	Inbound shock	Outbound shock
$\mathbf{B}_u$ (nT)	[−3.68, 0.13, 12.8]	[−3.60, 0.80, 13.0]
$\mathbf{B}_d$ (nT)	[−3.58, −0.50, 17.1]	[−3.61, −0.14, 16.7]
B_u (nT)	13.3	13.5
B_d (nT)	17.5	17.1
$R = B_d/B_u$	1.31	1.27
$\mathbf{V}_u$ (km/s)	[−357, 2, 12]	[−340, 11, 22]
$\mathbf{V}_d$ (km/s)	[−275, −35, 31]	[−278, −20, 37]
V_u (km/s)	357	342
V_d (km/s)	279	281
n_u (cm^{-3})	1.04	1.31
n_d (cm^{-3})	1.47	1.65
n_α/n_p	0.04	0.04
T_u (eV)	24.2	20.9
T_d (eV)	24.3	24.3
$\mathbf{v}_{sh}$ (km/s)	[7.6, −3.1, −0.7]	[−9.9, 4.5, 1.1]
V_{sh} (km/s)	8.3	10.9
$V_{a,u}$ (km/s)	270	244
$c_{s,u}$ (km/s)	60	56
$M_{A,u}$	1.25	1.24
$M_{ms,u}$	1.22	1.21
$\beta_{i,u}$	0.08	0.09
$\beta_{e,u}$	0.07	0.09
$\Omega_{i,u}$ (rad/s)	1.27	1.29
$\omega_{pi,u}$ (rad/s)	1340	1510
$r_{i,u}$ (ion convective gyro-radius; km)	265	233
$L_{i,u}$ (ion inertial length; km)	223	199
Shock ramp thickness ($L_{i,u}^{-1}$)	0.50	0.92
Cross-shock potential $s_{NIF} = e\phi/\frac{1}{2}m_iV_u^2$	0.36	0.50

Note. All values are for ions (unless otherwise indicated), calculated as averages for the upstream *u* and downstream *d* regions marked in Figure 4, and vectors are in geocentric solar ecliptic coordinates.

(McFadden, Carlson, Larson, Bonnell, et al., 2008), lead to upstream Alfvén and Magnetosonic Mach numbers in the range 1.2–1.25. The Mach numbers for these shocks are toward the lower end of the 1.2–1.5 range of estimated Alfvén Mach numbers for the shocks in Balikhin et al. (2008). The good agreement between the Mach numbers estimated from the magnetic compression and those calculated directly suggests that they are representative of the observed shocks. However, it should be noted that the directly calculated Mach numbers rely on the potentially unreliable density measurements. THEMIS-B (or Wind) density measurements indicate that the density and thus Mach numbers might be smaller, but at the same time, the THEMIS electrostatic analyzer underestimates the ion density in the solar wind (McFadden, Carlson, Larson, Ludlam, et al., 2008), potentially countering this effect. The ion and electron β values are in the range 0.07–0.09 for both shocks, so that the Alfvén Mach number is the dominant contributor to the Magnetosonic Mach number. As Venus Express plasma measurements were not available for the immediate time period investigated by Balikhin et al. (2008), nominal solar wind plasma parameters at 0.72 AU were assumed for the subsequent analysis. The availability of good quality plasma measurements at 1 AU allows a more accurate environment to be determined. In particular and despite the apparent unreliability of the density measurements, the low ion density in the magnetic cloud reduces the expected Mach numbers and β values

from those during typical solar wind conditions. For comparison, just upstream of the leading shock of the ICME, the Alfvén and Magnetosonic Mach numbers of the more nominal unshocked solar wind were 6.3 and 4.6 (calculated using the solar wind velocity in the direction of the inbound shock double coplanarity shock normal in Table 1), and the ion and electron β were 1.3 and 2.1, respectively.

THEMIS-C measures both the spin plane and axial electric field, allowing the cross-shock potential to be estimated. However, due to the short axial boom, only the spin plane electric field is measured with sufficient accuracy for low-frequency (<100 Hz) studies (Bonnell et al., 2008). For this reason, the spin plane electric field measurements are used, and the full three-component electric field across the shock is estimated based on its structure in the NIF (Dimmock et al., 2011, 2012). The cross-shock potential is calculated by integrating the change in the normal component of the electric field across the shock and multiplying this by the shock thickness calculated using the shock velocity determined from the downstream oscillations. The calculated shock thickness is 0.50 and 0.92 ion inertial lengths for the inbound and outbound shock, respectively, which is consistent with previous simulations of the shocks observed at Venus (Ofman et al., 2009). The resulting cross-shock potential is $s_{NIF} = 0.36$ for the inbound and $s_{NIF} = 0.50$ for the outbound shock. The cross-shock potential of very low Mach number shocks has not previously been studied in any detail using observations. Dimmock et al. (2012) studied the statistical dependence of the cross-shock potential for low Mach number shocks down to $M_A = 2$. This showed a general trend for the cross-shock potential to reduce as M_A increases, which is inline with theory. However, in the very low Mach number region, this trend should reverse, and the cross-shock potential should decrease with decreasing Mach number (Gedalin, 1997, 2017b; Gedalin & Balikhin, 2004). Using equations (12) and (23) in Gedalin (2017b), the predicted cross-shock potential is $s_{NIF} = 0.4$ for the inbound shock, with $M_A = 1.26$ and magnetic compression $R = 1.3$. For the outbound shock with $R = 1.27$, the Mach number should be accordingly lower. For $M_A = 1.23$ the theoretical prediction by Gedalin (2017b) gives $s_{NIF} = 0.38$. In both cases the agreement is rather good, given the observational uncertainties and the approximations made by Gedalin (2017b).

Based on their quasi-perpendicular structure, linearly polarized downstream oscillations, low magnetic compression, very low Mach number, and high altitude, these shock crossings observed in THEMIS-C data show the characteristics of the very low Mach number shocks in which kinematic effects dominate, which were previously observed in Venus Express magnetic field data.

3. Numerical Analysis Methodology

In order to compare the predictions of the collisionless relaxation theory with observations, we performed a test particle analysis of the motion of protons and α particles in a model shock front. In the analysis a shock is treated as one-dimensional and stationary. This is justified by the low Mach number and low β, as well as by the observations of a clean coherent profile of the magnetic field. The model magnetic field of a low-Mach number shock is taken as a monotonically increasing function of the coordinate along the shock normal. If x is along the shock normal and y is the noncoplanarity direction, then the main magnetic field is taken in the form of equations (6) and (7) (see, e.g., Gedalin, 2015).

$$B_z = B_u \sin\theta_{Bn}\left[1 + \frac{R-1}{2}\left(1 + \tanh\frac{3x}{D}\right)\right], \tag{6}$$

$$B_d/B_u = \sqrt{R^2\sin^2\theta_{Bn} + \cos^2\theta_{Bn}}. \tag{7}$$

The motional electric field $E_y = V_u B_u \sin\theta_{Bn}/c$ is constant throughout. The cross-shock electric field is chosen as $E_x \propto dB_z/dx$ (Gedalin & Balikhin, 2004) with the normalized cross-shock potential in the NIF, s_{NIF}, as a model parameter:

$$-e\int E_x dx = s_{NIF}(m_p V_u^2/2). \tag{8}$$

The noncoplanar magnetic field is also chosen $\propto dB_z/dx$ with the normalized de Hoffman-Teller cross-shock potential s_{HT} as a model parameter (Goodrich & Scudder, 1984; Schwartz et al., 1988).

$$e(V_u \tan\theta_{Bn}/c)\int B_y dx = (s_{NIF} - s_{HT})(m_p V_u^2/2) \tag{9}$$

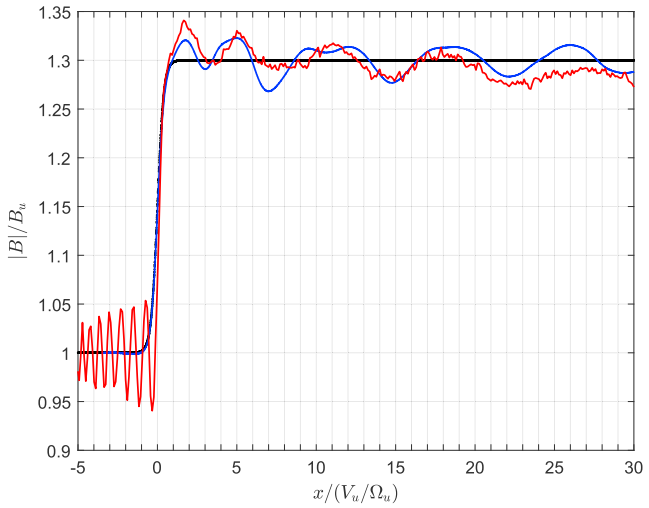

Figure 5. The model (black), numerically calculated (blue), and observed (red) magnetic field magnitudes for the inbound shock. The magnetic fields are normalized to their average upstream values and plotted against distance behind the shock in terms of ion convective gyro-radii.

The parameters θ_{Bn} and B_d/B_u are determined directly from the observations, while the parameters D, s_{NIF}, s_{HT}, and the Mach number M are varied to adjust the profile to the measured one (see below).

For each set of the parameters, protons and α-particles are numerically traced across the shock. Their upstream distributions are taken as Maxwellian, and the downstream pressures of the species are numerically calculated and used in the pressure balance equation (10) (Gedalin, 2017b), where $s = e, p, \alpha$. The total upstream pressure is given in equation (11), and the downstream electron pressure is taken as $p_{e,xx} = p_{e,u}(n_e/n_{e,u})^{\Gamma}$ with $\Gamma = 5/3$.

$$\sum_s p_{s,xx} + \frac{B^2}{8\pi} = p_t + p_B = p_u = \text{const}, \tag{10}$$

$$p_u = n_{p,u}m_pV_u^2 + n_{\alpha,u}m_\alpha V_u^2 + n_{p,u}T_{p,u} + n_{\alpha,u}T_{\alpha,u} + n_{e,u}T_{e,u} + \frac{B_u^2}{8\pi}. \tag{11}$$

The parameters T_s and $n_{s,u}$ are also taken from observations, although as previously noted, there are large uncertainties in these measurements.

Equation (10) is used to calculate the magnetic field magnitude B as a function of the coordinate x, to ensure that pressure balance is maintained. The shock parameters D, s_{NIF}, s_{HT}, and M are varied until the measured B_d/B_u is achieved asymptotically, and the calculated profile follows reasonably closely the model profile in the ramp region and the obtained downstream oscillations reasonably resemble the observed ones. It has been found (see also Gedalin, 2015) that the effects on the shock of D and the de Hoffman-Teller potential are minor, as well as the effects of the upstream temperature at these low upstream v_T/V_u. Here v_T is the upstream thermal velocity of an ion species. According to the recent review by Wilson III et al. (2018), the temperature ratio T_α/T_p varies in the solar wind with a mean value of around 2. The ratio of the thermal speeds varies approximately in the range $v_{T\alpha}/v_{Tp} \approx 0.5 - 1$. As has been previously shown by Gedalin (2015), the effect of the temperature depends on the ratio $v_T/V_u\sqrt{1-(Q_p/Q)s_{NIF}}$, where $Q = m/q$ is the mass-to-charge ratio of the species. Namely, for α particles this ratio is $v_{T\alpha}/V_u\sqrt{1-s_{NIF}/2}$, which remains small for the measured β_i even for $v_{T\alpha}/v_{Tp} = 2$. This means that α particles essentially behave as cold at the scales under study and the precise value of β_α, used in the numerical analysis, has no effect.

4. Results and Discussion

Figure 5 shows the magnitudes of the model (black) magnetic field, the magnetic field calculated from equation (10) (blue), and the observed magnetic field for the inbound shock (red). The time for the observed magnetic field is converted into distance behind the shock using the shock velocity determined from the downstream oscillations and shifted to match the ramp location of the calculated profile. Given the uncertainties of our knowledge of the shock structure, the agreement is surprisingly good. The Alfvén Mach number for the calculated shock is $M_a = 1.26$, while the cross-shock potential $s_{NIF} = 0.37$. This compares very closely to the values of $M_a = 1.25$ and $s_{NIF} = 0.26$ measured for the inbound shock. The values of both parameters are also in good agreement with previous theoretical predictions (Gedalin, 2017b).

As is evident from Figure 5, the observed relative scales are in good agreement with the theoretical predictions. Translation of relative scales into kilometers is not easy because of the unreliable density measurements. However, using the previously derived shock velocity calculated from the first downstream oscillation, the density jump across the shock can be estimated using the mass-flux conservation applied across the shock (Schwartz, 1998). This leads to a value of $n_d/n_u = 1.34$, which is consistent with the $n_d/n_u = 1.32$ produced in the numerical analysis. The observed ramp is steeper than the model one, due to the upstream precursor, which is not included in the theoretical analysis. The model ramp width slightly affects the position of the downstream peaks but has almost no effect on the amplitude of the downstream oscillations. As the analysis shows excellent agreement to the observations in the downstream region without including the upstream precursor in the model, its effect on the downstream ion distributions is relatively unimportant.

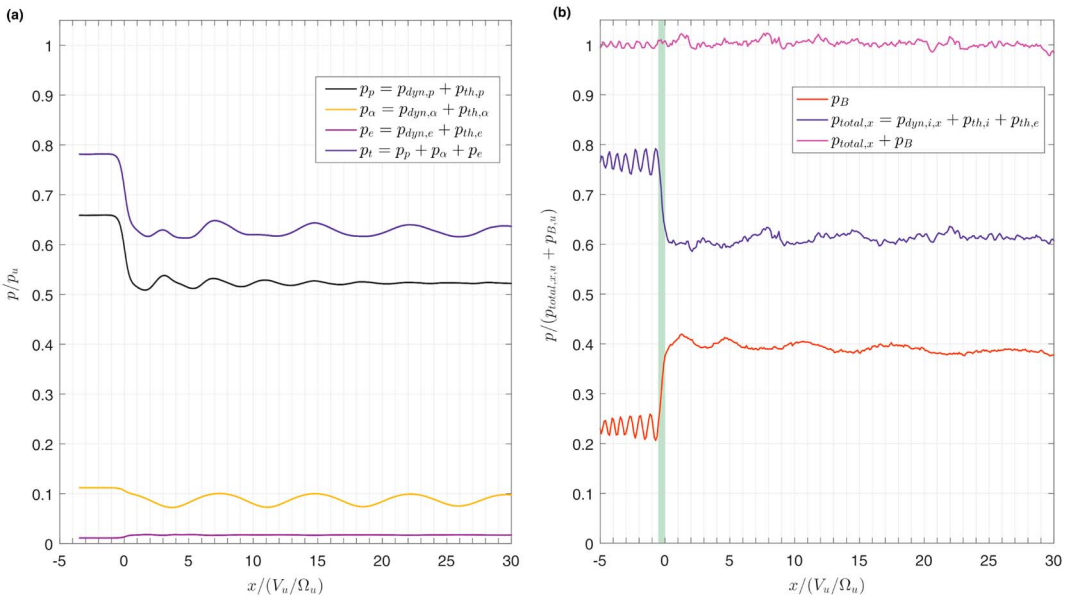

Figure 6. (a) Downstream pressures of all species (proton, black; α particle, yellow; electron, purple) and the total downstream pressure (blue) of the plasma resulting from numerical analysis of the theoretical particle motion of a shock with parameters similar to the observed inbound shock; (b) THEMIS-C pressures for the inbound shock: magnetic pressure (red), total plasma pressure calculated assuming mass conservation across the shock (blue), and total pressure (magneta). All values are normalized to the upstream average total pressure and plotted against distance behind the shock in terms of ion convective gyro-radii. The green region in (b) marks the main shock ramp.

In this case the ratio $n_{\alpha,u}/n_{p,u} = 0.04$, which is consistent with the Wind observations in Figure 3. A rough estimate of the downstream gyration speed gives $V_u(\sqrt{1 - s_{NIF}} - B_u/B_d)$ for protons and $V_u(\sqrt{1 - s_{NIF}/2} - B_u/B_d)$ for α particles (Gedalin et al., 2015). Therefore, the effect of the cross-shock potential on the variations of the downstream pressure of α particles is weak, while for protons s_{NIF} is the main parameter, which controls the downstream pressure variations for a given B_d/B_u. The damping distance of the oscillations, due to the gyrophase mixing, rapidly decreases with the increase of v_T/V_u (Gedalin, 2015). If the upstream proton and α-particle temperatures are nearly equal, this ratio is twice as large for the protons than for the α particles. Therefore, the oscillations of the downstream proton pressure damps much faster than that of the α particles. For the measured parameters of the inbound shock, the proton pressure oscillations damp quickly, so that they are seen only just behind the ramp: The distance between the first two peaks is about $3.5(V_u/\Omega_u) \approx 2\pi(V_u/\Omega_u)/(B_d/B_u)^2$, as predicted by theory (Balikhin et al., 2008; Gedalin et al., 2015; Ofman et al., 2009). The wavelength for the farther oscillations is twice as large, which shows that they are due to the α particles. This is clearly seen in Figure 6a, which shows the pressures of all species and the total pressure. There is no noticeable effect of s_{HT} in the numerical analysis for this shock.

Figure 6a shows the downstream oscillations in the numerically derived plasma pressures. The magnetic pressure in the numerical analysis (not shown) is calculated directly using the total plasma pressure to ensure balance, $p_B = p_u - p_t$, and as such will inherently show out-of-phase oscillations with the total plasma pressure. Due to the inaccuracy of the THEMIS-C ion density data for the observation period, the dynamic pressure calculated directly from the observed ion density and velocity and consequently the on-board-derived ion-pressure moment are unreliable. Instead, under the condition of mass conservation across the shock, the dynamic pressure can be estimated by $p_{dyn,i,x} = n_u m_i V_{u,x} V_x$ (Balikhin et al., 2008; Ofman et al., 2009). Using this estimate, the total plasma pressure can be calculated as $p_{total,x} = p_{dyn,i,x} + p_{th,i} + p_{th,e}$. This is plotted together with the magnetic pressure $p_B = B^2/2\mu_0$ in Figure 6b for the inbound shock crossing and assuming a two particle fluid with $n_\alpha/n_p = 0.04$. The total pressure shows the expected downstream oscillations that slowly decay in magnitude and that are out of phase with the oscillations in the magnetic pressure, as predicted by the theory for kinematic relaxation. The oscillations in the observed total plasma pressure in Figure 6b compare very favorably with the oscillations in the total plasma pressure from the numerical analysis in Figure 6a, both in terms of their magnitude and the locations of the maxima/minima of each period. This confirms the role of both the protons and α particles in forming the

ion distribution and magnetic field profile downstream of the shock. The downstream oscillations observed in the total pressure predominantly arise due to the gyration of the ions in the shock normal direction and can be clearly seen in the component of the ion velocity in the shock normal direction, which is plotted in Figure 3b. The result is a near constant total pressure, plotted as the magenta line in Figure 6b, downstream of the ramp. The outbound shock (not shown) shows similar characteristics in terms of antiphase oscillation in the total plasma and magnetic pressure. However, the oscillations do not show the change in period due to a fast decay of the proton oscillations. Instead, the higher cross-shock potential when compared to the inbound shock increases the amplitude and damping length of the oscillations in the proton distribution, such that their effect dominates in the downstream ion distribution.

Linearly polarized changes in the magnetic field due to the mirror mode are commonly observed in experimental data and simulation downstream of the terrestrial bow shock (e.g., Dimmock et al., 2015; McKean et al., 1996; Soucek et al., 2008; Soucek & Escoubet, 2011; Tsurutani et al., 2011). They can be generated near the bow shock and convected downstream further into the magnetosheath. However, the mirror mode can be ruled out as the cause of the oscillations downstream of these very low Mach number shocks, since the observed anticorrelation in Figure 6b occurs between the magnetic and total plasma pressure, as opposed to between the magnetic and thermal pressure. In addition, the mirror mode is unstable for high β plasmas. In the region immediately behind these observed shocks, the ion and electron plasma β are both low (<0.1), and as a result, the mirror mode instability condition, which requires $\beta_{\perp}(T_{\perp}/T_{\parallel} - 1) > 1$ (Soucek & Escoubet, 2011), is not met ($\beta_{\perp}(T_{\perp}/T_{\parallel} - 1) \ll 1$). An alternative and commonly used explanation for oscillations downstream of quasi-perpendicular shocks is ion-cyclotron waves related to an ion-pressure anisotropy (e.g., McKean et al., 1995, 1996; Remya et al., 2014). These are usually observed as transverse circularly polarized waves in the magnetic field, and thus, the linear polarization of the observed oscillations rules this out. However, the ion-cyclotron instability can generate linearly (or nearly linear) polarized waves when the left and right-hand branches of the dispersion curve generate waves with the same (or very similar amplitude) (Stringer, 1963). For the observed linearly polarized oscillations the temperature anisotropy ($T_{\perp}/T_{\parallel} < 2$) is relatively modest, which coupled to the low β would lead to a very small growth rate for the ion-cyclotron instability (Gary, 1992).

The shocks occur at an altitude of 57.7 R_E and Sun-Earth-satellite angle $\theta = 57°$. This compares to 11.4 R_E and $\theta = 28°$ for the first Cluster 2 bow shock crossing when the cloud phase commences and 20.6 R_E and $\theta = 35°$ for the first Cluster 2 bow shock crossing after the THEMIS-C shock crossings. An altitude of 57.7 R_E at $\theta = 57°$ would be abnormally high for the Earth's bow shock, but it is not unprecedented. Formisano et al. (1971) observed the Earth's bow shock numerous times at high altitudes (e.g., 32.5 R_E at $\theta = 45°$), while Fairfield et al. (2001) made numerous comparable observations (e.g., 51 R_E at $\theta = 31°$ and 58 R_E at $\theta = 53°$), which were supported with comparison to model positions. In both of these studies the observed high altitude shocks were generally associated with unusually low solar wind densities. The refined bow shock model in Jeráb et al. (2005) has been shown to accurately predict the location of the bow shock under varying solar wind conditions, in particular for low M_A. Using this model and the solar wind parameters determined for the inbound shock listed in Table 2, the predicted location of the bow shock at the Sun-Earth-satellite observation angle is [34, −52, 4] R_E. This is very close to the observation location of [32, −49, 4] R_E and indicates that the observed shock was highly likely to be the Earth's bow shock.

5. Conclusion

Quasi-perpendicular shocks in which kinematic relaxation of the nongyrotropic ion population downstream is the dominant process for energy redistribution have previously only been observed at the Venusian bow shock and for interplanetary shocks. In this paper, plasma and magnetic field measurements from the THEMIS spacecraft are used, together with numerical analysis, to study this shock structure near the Earth for the first time. The observed shock occurred during the very low Mach number magnetic cloud phase of an ICME. The main results of the study can be summarized as follows:

1. A very good agreement between the theoretically (numerically derived) predicted shock profile and the observed one.
2. Observational confirmation of the anticorrelation of the ion and magnetic pressure.
3. Close similarity between the derived pressure dependencies and the observed ones.
4. The ability of theory to improve observational analysis when some measurements are unreliable.

5. The first direct confirmation of kinematic collisionless relaxation for the formation of the downstream ion distributions.
6. Confirmation of the stationarity and one dimensionality of the observed shock.
7. Clear identification of the proton and α-particle contribution and the first direct confirmation of the significance of α particles in the formation of the shock structure.
8. Insignificance of the upstream precursor in the formation of the downstream ion distributions.
9. Evidence to suggest that the observed shock might be a crossing of the Earth's distant bow shock due to the very low magnetosonic and Alfvén Mach numbers in the magnetic cloud.

The process of kinematic relaxation of the nongyrotropic ion population downstream of a quasi-perpendicular shock should occur at all Mach numbers. As such, the close agreement between observation and theory shown in this paper should aid in providing future insight into the energy redistribution processes at shocks of all Mach numbers, not just very low Mach numbers.

Acknowledgments
M. G. was supported in part by the Israel Science Foundation (Grant 368/14). M. A. B. was supported by STFC Consolidator Grant ST/R000697/1. We acknowledge NASA contract NAS5-02099 and V. Angelopoulos for use of data from the THEMIS Mission, specifically K. H. Glassmeier, U. Auster, and W. Baumjohann for the use of FGM data provided under the lead of the Technical University of Braunschweig and with financial support through the German Ministry for Economy and Technology and the German Center for Aviation and Space (DLR) under contract 50 OC 0302, C. W. Carlson and J. P. McFadden for use of ESA data, and J. W. Bonnell and F. S. Mozer for use of EFI data. We acknowledge the Wind SWE team and use of associated data. THEMIS and WIND data are available through the NASA Coordinated Data Analysis Web (CDAWeb) service (https://cdaweb.sci.gsfc.nasa.gov). Cluster data are available through the Cluster Data Archive (CSA) (https://csa.esac.esa.int).

References

Angelopoulos, V. (2011). The ARTEMIS mission. *Space Science Reviews*, *165*(1), 3–25.
Balikhin, M. A., Zhang, T. L., Gedalin, M., Ganushkina, N. Y., & Pope, S. A. (2008). Venus express observes a new type of shock with pure kinematic relaxation. *Geophysical Research Letters*, *35*, L01103. https://doi.org/10.1029/2007GL032495
Balogh, A., Schwartz, S., Bale, S., Balikhin, M., Burgess, D., Horbury, T., et al. (2005). Cluster at the bow shock: Introduction, *Outer magnetospheric boundaries: Cluster results* (pp. 155–160). Dordrecht: Springer.
Bonnell, J. W., Mozer, F. S., Delory, G. T., Hull, A. J., Ergun, R. E., Cully, C. M., et al. (2008). The electric field instrument (EFI) for THEMIS. *Space Science Reviews*, *141*(1-4), 303–341.
Burch, J. L., Moore, T. E., Torbert, R. B., & Giles, B. L. (2016). Magnetospheric multiscale overview and science objectives. *Space Science Reviews*, *199*(1-4), 5–21.
Burgess, D., Wilkinson, W., & Schwartz, S. (1989). Ion distributions and thermalization at perpendicular and quasi-perpendicular supercritical collisionless shocks. *Journal of Geophysical Research*, *94*(A7), 8783–8792.
Burlaga, L., Sittler, E., Mariani, F., & Schwenn, R. (1981). Magnetic loop behind an interplanetary shock: Voyager, Helios, and IMP 8 observations. *Journal of Geophysical Research*, *86*(A8), 6673–6684.
Chai, L., Wan, W., Fraenz, M., Zhang, T., Dubinin, E., Wei, Y., et al. (2015). Solar zenith angle-dependent asymmetries in venusian bow shock location revealed by venus express. *Journal of Geophysical Research: Space Physics*, *120*, 4446–4451. https://doi.org/10.1002/2015JA021221
Dimmock, A. P., Balikhin, M. A., & Hobara, Y. (2011). Comparison of three methods for the estimation of cross-shock electric potential using cluster data. *Annales Geophysicae*, *29*(5), 815–822.
Dimmock, A. P., Balikhin, M. A., Krasnoselskikh, V. V., Walker, S. N., Bale, S. D., & Hobara, Y. (2012). A statistical study of the cross-shock electric potential at low mach number, quasi-perpendicular bow shock crossings using cluster data. *Journal of Geophysical Research*, *117*, 2156–2202. https://doi.org/10.1029/2011JA017089
Dimmock, A. P., Osmane, A., Pulkkinen, T. I., & Nykyri, K. (2015). A statistical study of the dawn-dusk asymmetry of ion temperature anisotropy and mirror mode occurrence in the terrestrial dayside magnetosheath using THEMIS data. *Journal of Geophysical Research: Space Physics*, *120*, 5489–5503. https://doi.org/10.1002/2015JA021192
Fairfield, D. H., Iver, H. C., Desch, M. D., Szabo, A., Lazarus, A. J., & Aellig, M. R. (2001). The location of low mach number bow shocks at Earth. *Journal of Geophysical Research*, *106*(A11), 25,361–25,376. https://doi.org/10.1029/2000JA000252
Farris, M. H., Russell, C. T., & Thomsen, M. F. (1993). Magnetic structure of the low beta, quasi-perpendicular shock. *Journal of Geophysical Research*, *98*(A9), 15,285–15,294.
Formisano, V., Hedgecock, P. C., Moreno, G., Sear, J., & Bollea, D. (1971). Observations of Earth's bow shock for low mach numbers. *Planetary and Space Science*, *19*(11), 1519–1531.
Galeev, A. A. (1976). Collisionless shocks. In D. J. Williams (Ed.), *Physics of solar planetary environments* pp. 464–490). Colorado.
Galeev, A. A., Gal'Perin, Y. I., & Zelenyj, L. M. (1996). The INTERBALL project to study solar-terrestrial physics. *Kosmicheskie Issledovaniia*, *34*, 339–362.
Gary, S. P. (1992). The mirror and ion cyclotron anisotropy instabilities. *Journal of Geophysical Research*, *97*(A6), 8519–8529. https://doi.org/10.1029/92JA00299
Gedalin, M. (1996). Transmitted ions and ion heating in nearly perpendicular low-mach number shocks. *Journal of Geophysical Research*, *101*(15), 569. https://doi.org/10.1029/96JA00924
Gedalin, M. (1997). Ion heating in oblique low-Mach number shocks. *Geophysical Research Letters*, *24*(20), 2511–2514.
Gedalin, M. (2015). Collisionless relaxation of non-gyrotropic downstream ion distributions: Dependence on shock parameters. *Journal of Plasma Physics*, *81*(06), 12.
Gedalin, M. (2016). Transmitted, reflected, quasi-reflected, and multiply reflected ions in low-Mach number shocks. *Journal of Geophysical Research: Space Physics*, *121*, 10,754–10,767. https://doi.org/10.1002/2016JA023395
Gedalin, M. (2017a). Effect of alpha particles on the shock structure. *Journal of Geophysical Research: Space Physics*, *122*, 71–76. https://doi.org/10.1002/2016JA023460
Gedalin, M. (2017b). Rankine-Hugoniot relations in multispecies plasma with gyrotropic anisotropic downstream ion distributions. *Journal of Geophysical Research: Space Physics*, *122*, 11,857–11,863. https://doi.org/10.1002/2017JA024757
Gedalin, M., & Balikhin, M. A. (2004). Electric potential in the low-Mach-number quasi-perpendicular collisionless shock ramp revisited. *Journal of Geophysical Research*, *109*, A03106. https://doi.org/10.1029/2003JA010219
Gedalin, M., Friedman, Y., & Balikhin, M. (2015). Collisionless relaxation of downstream ion distributions in low-Mach number shocks. *Physics of Plasmas*, *22*(7), 072301. https://doi.org/10.1063/1.4926452
Goncharov, O., Šafránková, J., Nemecek, Z., Prech, L., Pitna, A., & Zastenker, G. N. (2014). Upstream and downstream wave packets associated with low-Mach number interplanetary shocks. *Geophysical Research Letters*, *41*, 8100–8106. https://doi.org/10.1002/2014GL062149

Goodrich, C. C., & Scudder, J. D. (1984). The adiabatic energy change of plasma electrons and the frame dependence of the cross-shock potential at collisionless magnetosonic shock waves. *Journal of Geophysical Research*, *89*(A8), 6654–6662. https://doi.org/10.1029/JA089iA08p06654

Greenstadt, E. W., & Mellott, M. M. (1987). Plasma wave evidence for reflected ions in front of subcritical shocks: ISEE 1 and 2 observations. *Journal of Geophysical Research*, *92*(A5), 4730–4734. https://doi.org/10.1029/JA092iA05p04730

Helder, E., Vink, J., Bykov, A., Ohira, Y., Raymond, J., & Terrier, R. (2012). Observational signatures of particle acceleration in supernova remnants. *Space Science Reviews*, *173*(1-4), 369–431.

Jeráb, M., Nemecek, Z., Šafránková, J., Jelínek, K., & Merka, J. (2005). Improved bow shock model with dependence on the IMF strength. *Planetary and Space Science*, *53*(1-3), 85–93. https://doi.org/10.1016/j.pss.2004.09.032

Kajdič, P., Blanco-Cano, X., Aguilar-Rodriguez, E., Russell, C. T., Jian, L. K., & Luhmann, J. G. (2012). Waves upstream and downstream of interplanetary shocks driven by coronal mass ejections. *Journal of Geophysical Research*, *117*, A06103. https://doi.org/10.1029/2011JA017381

Kennel, C. F., Edmiston, J. P., & Hada, T. (1985). A quarter century of collisionless shock research. In C. F. Kennel, J. P. Edmiston, & T. Hada (Eds.), *Collisionless shocks in the heliosphere: A tutorial review, Geophysical Monograph Series* (Vol. 34, pp. 1–36). Washington, DC: American Geophysical Union.

Leamon, R. J. (2002). Properties of magnetic clouds and geomagnetic storms associated with eruption of coronal sigmoids. *Journal of Geophysical Research*, *107*(A9), 1234. https://doi.org/10.1029/2001JA000313

Lu, Q., Shan, L., Zhang, T., Zank, G. P., Yang, Z., Wu, M., et al. (2013). The role of pickup ions on the structure of the venusian bow shock and its implications for the termination shock. *The Astrophysical Journal*, *773*(2), L24. https://doi.org/10.1088/2041-8205/773/2/L24

McEnulty, T., Luhmann, J., de Pater, I., Brain, D., Fedorov, A., Zhang, T., & Dubinin, E. (2010). Interplanetary coronal mass ejection influence on high energy pick-up ions at venus. *Planetary and Space Science*, *58*(14-15), 1784–1791. https://doi.org/10.1016/j.pss.2010.07.019

McFadden, J. P., Carlson, C. W., Larson, D., Bonnell, J., Mozer, F., Angelopoulos, V., et al. (2008). THEMIS, ESA first science results and performance issues. *Space Science Reviews*, *141*(1-4), 477–508. https://doi.org/10.1007/s11214-008-9433-1

McFadden, J. P., Carlson, C. W., Larson, D., Ludlam, M., Abiad, R., Elliott, B., et al. (2008). The THEMIS ESA plasma instrument and in-flight calibration. *Space Science Reviews*, *141*(1-4), 277–302. https://doi.org/10.1007/s11214-008-9440-2

McKean, M. E., Omidi, N., & Krauss-Varban, D. (1995). Wave and ion evolution downstream of quasi-perpendicular bow shocks. *Journal of Geophysical Research*, *100*(A3), 3427–3437.

McKean, M. E., Omidi, N., & Krauss-Varban, D. (1996). Magnetosheath dynamics downstream of low mach number shocks. *Journal of Geophysical Research*, *101*(A9), 20,013–20,022. https://doi.org/10.1029/96JA01461

Mellott, M. (1985). Subcritical collisionless shock waves, *Collisionless shocks in the heliosphere: Reviews of current research* (pp. 131–140). Washington: AGU.

Ofman, L., Balikhin, M., Russell, C. T., & Gedalin, M. (2009). Collisionless relaxation of ion distributions downstream of laminar quasi-perpendicular shocks. *Journal of Geophysical Research*, *114*, A09106. https://doi.org/10.1029/2009JA014365

Ofman, L., & Gedalin, M. (2013). Two-dimensional hybrid simulations of quasi-perpendicular collisionless shock dynamics: Gyrating downstream ion distributions. *Journal of Geophysical Research: Space Physics*, *118*, 1828–1836. https://doi.org/10.1029/2012JA018188

Ogilvie, K. W., von Rosenvinge, T., & Durney, A. C. (1977). International Sun-Earth explorer: A three-spacecraft program. *Science*, *198*(4313), 131–138. https://doi.org/10.1126/science.198.4313.131

Peredo, M., Slavin, J. A., Mazur, E., & Curtis, S. A. (1995). Three-dimensional position and shape of the bow shock and their variation with alfvĀlnic, sonic and magnetosonic mach numbers and interplanetary magnetic field orientation. *Journal of Geophysical Research*, *100*(A5), 7907–7916. https://doi.org/10.1029/94JA02545

Remya, B., Tsurutani, B. T., Reddy, R. V., Lakhina, G. S., Falkowski, B. J., Echer, E., & Glassmeier, K.-H. (2014). Large-amplitude electromagnetic proton cyclotron waves throughout the Earth's magnetosheath: Cassini and wind observations. *The Astrophysical Journal*, *793*(1), 6. https://doi.org/10.1088/0004-637X/793/1/6

Russell, C. T. (1985). Planetary Bow Shocks. In *Collisionless shocks in the heliosphere: Reviews of current research* (pp. 109–130). Washington, DC: American Geophysical Union. https://doi.org/10.1029/GM035p0109

Russell, C. T., Elphic, R. C., & Slavin, J. A. (1979). Pioneer magnetometer observations of the venus bow shock. *Nature*, *282*, 815.

Russell, C. T., Jian, L. K., Blanco-Cano, X., & Luhmann, J. G. (2009). Stereo observations of upstream and downstream waves at low Mach number shocks. *Geophysical Research Letters*, *36*, L03106. https://doi.org/10.1029/2008GL036991

Schure, K., Bell, A., Drury, L., & Bykov, A. (2012). Diffusive shock acceleration and magnetic field amplification. *Space Science Reviews*, *173*(1-4), 491–519.

Schwartz, S. J. (1998). Shock and discontinuity normals, mach numbers, and related parameters. *ISSI Scientific Reports Series*, *1*, 249–270.

Schwartz, S. J., Thomsen, M. F., Bame, S. J., & Stansberry, J. (1988). Electron heating and the potential jump across fast mode shocks. *Journal of Geophysical Research*, *93*(A11), 12,923–12,931. https://doi.org/10.1029/JA093iA11p12923

Scudder, J. D. (1995). A review of the physics of electron heating at collisionless shocks. *Advances in Space Research*, *15*(8-9), 181–223.

Scudder, J. D., Mangeney, A., Lacombe, C., Harvey, C. C., Aggson, T. L., Anderson, R. R., et al. (1986). The resolved layer of a collisionless, high β, supercritical, quasi-perpendicular shock wave: 1. Rankine-Hugoniot geometry, currents, and stationarity. *Journal of Geophysical Research*, *91*(A10), 11,019–11,052.

Sibeck, D. G., & Angelopoulos, V. (2008). THEMIS, science objectives and mission phases. *Space Science Reviews*, *141*(1-4), 35–59.

Soucek, J., & Escoubet, C. P. (2011). Cluster observations of trapped ions interacting with magnetosheath mirror modes. *Annales Geophysicae*, *29*(6), 1049–1060. https://doi.org/10.5194/angeo-29-1049-2011

Soucek, J., Lucek, E., & Dandouras, I. (2008). Properties of magnetosheath mirror modes observed by cluster and their response to changes in plasma parameters. *Journal of Geophysical Research*, *113*, A04203. https://doi.org/10.1029/2007JA012649

Stringer, T. E. (1963). Low-frequency waves in an unbounded plasma. *Journal of Nuclear Energy. Part c, Plasma Physics, Accelerators, Thermonuclear Research*, *5*(2), 89.

Tsurutani, B. T., Lakhina, G. S., Verkhoglyadova, O. P., Echer, E., Guarnieri, F. L., Narita, Y., & Constantinescu, D. O. (2011). Magnetosheath and heliosheath mirror mode structures, interplanetary magnetic decreases, and linear magnetic decreases: Differences and distinguishing features. *Journal of Geophysical Research*, *116*, A02103. https://doi.org/10.1029/2010JA015913

Van Weeren, R. J., Rottgering, H. J. A., Bruggen, M., & Hoeft, M. (2010). Particle acceleration on megaparsec scales in a merging galaxy cluster. *Science*, *330*(6002), 347–349.

Vech, D., Szego, K., Opitz, A., Kajdic, P., Fraenz, M., Kallio, E., & Alho, M. (2015). Space weather effects on the bow shock, the magnetic barrier, and the ion composition boundary at venus. *Journal of Geophysical Research: Space Physics*, *120*, 4613–4627. https://doi.org/10.1002/2014JA020782

Wilson III, L. B., Stevens, M. L., Kasper, J. C., Klein, K. G., Maruca, B. A., Bale, S. D., et al. (2018). The statistical properties of solar wind temperature parameters near 1 AU. *The Astrophysical Journal Supplement Series*, *236*(2), 41. https://doi.org/10.3847/1538-4365/aab71c

Zhang, T. L., Pope, S., Balikhin, M., Russell, C. T., Jian, L. K., Volwerk, M., et al. (2008). Venus Express observations of an atypically distant bow shock during the passage of an interplanetary coronal mass ejection. *Journal of Geophysical Research*, *113*, E00B12. https://doi.org/10.1029/2008JE003128

Zilbersher, D., Gedalin, M., Newbury, J. A., & Russell, C. T. (1998). Direct numerical testing of stationary shock model with low mach number shock observations. *Journal of Geophysical Research*, *103*(26), 775. https://doi.org/10.1029/98JA02464